Kinetics and Mechanism of Emulsifier-Free Emulsion Polymerization: Styrene/Hydrophilic Comonomer (Acrylamide) System

Show-An Chen* and Song-Tai Lee

Chemical Engineering Department, National Tsing-Hua University, Hsinchu, Taiwan 30043, China

Received July 17, 1989; Revised Manuscript Received December 21, 1990

ABSTRACT: For the emulsifier-free emulsion polymerization of styrene with a minor amount of acrylamide as water-soluble comonomer and potassium persulfate as initiator, experimental studies on the kinetics, molecular weight distributions, and particle morphology have been carried out. It was found that the particle nucleation is likely to yield primary particles via the mechanism of homogeneous coagulative nucleation and coagulation of the primary particles to yield uniform particles. The particle growth in the postnucleation stage is via a shell growth mechanism, by which the polymerization occurs mainly in the shell region with a thickness equal to the root-mean-square end-to-end distance of the growing polymers (about 100–400 Å in thickness). The particles are considered to be uniformly saturated with monomer before disappearance of the monomer droplets. On the premise of the combination termination mechanism of the growing radicals, the shell reaction characteristic in the present systems is due to surface anchoring of the sulfate ends of the growing radicals and to the large size of the particle (greater than twice its end-to-end distance, ca. 1500–2000 Å in diameter). The average number of growing radicals per particle in the growth period is found to be from two to six, much higher than that in the conventional case. The high $\bar{n}$ value and confined polymerization in the shell region cause a termination of the growing radicals at lower molecular weight (MW), on the order of 10^4–10^5. This lower MW is consistent with the calculated shell thickness, since the growing chain end must locate within the shell having a thickness equal to its end-to-end distance.

Introduction

Emulsifier-free emulsion polymerization can be used to synthesize particles having functional groups exposed on the surface for biomedical and catalytic support applications and latexes having no surfactant migration after film forming for coating and adhesive applications.

For improving stability of the emulsion or incorporating functional groups on the particle surface, a minor amount of hydrophilic ionic or nonionic comonomer (less than 5 mol % of total monomer) is added in the system styrene (St)/potassium persulfate (KPS)/water. Systems with ionic comonomers were reviewed in our previous works,[1-4] while systems with nonionic comonomers (or weak acid or weak base), which involve 2-hydroxyethyl methacrylate (HEMA), acrylamide (AAm), and acrylic acid (AA), are of particular interest in this work and are reviewed below.

For the system St/HEMA/KPS/water, Chen and Chang[5] observed an apparent linearity of (conversion)$^{2/3}$ against time for conversions up to about 40% and considered that the particle, which consists of a rigid core, grows due to shell region polymerization. However, no direct evidence was provided to support existence of the rigid core and shell region reaction during the postnucleation stage. For the system St/AAm/KPS/water, Ohtsuka et al.[6] used a high AAm content (up to 67 mol %) and proposed a three-stage scheme for consumption of the monomers. Tamai et al.[7] also found that only about one-sixth of AAm could copolymerize with the styrene monomer. Ceska[8] used AA as the comonomer in the preparation of styrene/butadiene copolymer particles. However, these works made no attempt to explore the particle growth mechanism.

In regard to the nucleation mechanism, for emulsifier-free systems of styrene, the presence of oligomers seems to favor the micellar mechanism,[9] while the variation of particle number density (N_p) with initiator concentration and ionic strength seems to favor the coagulative nucleation mechanism.[10,11] For systems of styrene with ionic comonomers, however, it is sometimes suggested to follow the micellar nucleation mechanism or a combination of the micellar and coagulation mechanisms.[1,2]

The objective of this work is to clarify the mechanisms of particle nucleation and growth for the emulsifier-free system St/AAm/KPS/water.

Experimental Section

Materials. Styrene was used after purification by the usual method.[1] Water was fresh deionized. Acrylamide (AAm) and potassium persulfate (KPS) were recrystallized from benzene and deionized water, respectively. The chemicals sodium sulfate, isoprene, tetrahydrofuran (THF), sodium lauryl sulfate (SLS), and azobis(isobutyronitrile) (AIBN) were used as received from Merck Co. The epoxy resin (Epon 812), its curing agent (2,4-bis(dimethylamino)-6-methylphenol), and osmium tetroxide were used as received from Electron Microscopy Science Co.

Polymerization Procedure and Particle Characterization. Emulsion polymerizations were carried out at 70 ± 0.5 °C in a 500-mL four-neck receptor purged with nitrogen continuously. The reactor was equipped with a Teflon mixer, condenser, thermocouple, and a rubber septum caped on one neck for taking samples. The agitation speed for all runs was 200 ± 20 rpm. The recipes of all runs are listed in Table I.

The samples withdrawn from the reactor were first exposed to air, quenched in an ice/water bath, and then vacuum-dried without heating for determination of conversion curves. Although no inhibitor was added, it was found that addition of the inhibitor, hydroquinone, into the samples before drying provided no additional inhibition effect in the determination of conversion. Molecular weight distributions (MWDs) were measured by use of GPC with dual detectors for comparison, an UV detector at the wavelength of 254 nm, and a refractive index (RI) detector. The columns used were two Ultrastyragel columns (Waters Co.) in series having the regular MW exclusion limit from 2000 to 10^6. The flow rate of the carrier solvent, THF, was 1 mL/min. However, for identification of MWDs of oligomers, columns A-801 and 803 (Shodex Co.) in series having the MW exclusion limit from 10 to 7×10^4 were used. Particle diameter ($\bar{D}_p$) and particle

* Author to whom correspondence should be addressed.

0024-9297/91/2224-3340$02.50/0

Table I
Recipes and Characteristic Values of the Emulsifier-Free Emulsion Polymerization Runs at 70 °C

	A series					K series					
parameter	A1	A2	A3	A4	A5	K1	K2 (A3)	K3	K4	K5	K6
polymerization recipes											
styrene, g	50.00	50.00	50.00	50.00	50.00	50.00	50.00	50.00	50.00	50.00	50.00
acrylamide, g	0.00	0.20	0.40	0.80	1.60	0.40	0.40	0.40	0.40	0.40	0.40
KPS, g	0.50	0.50	0.50	0.50	0.50	0.25	0.50	0.75	1.00	1.50	2.00
water, g	400.00	400.00	400.00	400.00	400.00	400.00	400.00	400.00	400.00	400.00	400.00
Na_2SO_4, g											
ionic strength, mol/L of H_2O	0.014	0.014	0.014	0.014	0.014	0.007	0.014	0.021	0.028	0.042	0.055
limiting conv[a]	0.92	0.95	0.98	0.99	0.96	0.98	0.98	0.98	0.98	0.99	1.00
$\bar{M}_n$, 10^4	5.59	4.84	4.62	4.67	6.25	6.03	4.62	3.16	3.19	2.60	2.80
$\bar{M}_w$, 10^5	3.07	2.96	2.72	2.55	2.83	4.39	2.72	1.79	1.84	1.31	1.11
D_p by TEM, 10^3 Å	5.40	5.10	4.90	4.70	4.50	4.00	4.90	7.60	5.40	4.70	4.50
N_p by TEM, 10^{12}/cm^3 of H_2O	1.33	1.64	1.91	2.20	2.46	3.48	1.91	0.52	1.44	2.22	2.59
N_p by scattering, 10^{12}/cm of H_2O	1.07	1.46	1.80	1.62	1.69		1.80	0.41	1.05	1.32	2.06
shell thickness (L), Å	155	238	225	313	391	261	225	413	205	250	263
av shell thickness, Å[b]			250			250	250	250	250	250	250

	J series				I series			
parameter	J1	J2	J3	J4 (K6)	I1 (A3)	I2	I3	I4
polymerization recipes								
styrene, g	50.00	50.00	50.00	50.00	50.00	50.00	50.00	50.00
acrylamide, g	0.40	0.40	0.40	0.40	0.40	0.40	0.40	0.40
KPS, g	0.50	1.00	1.50	2.00	0.50	0.50	0.50	0.50
water, g	400.00	00.00	400.00	400.00	400.00	400.00	400.00	400.00
Na_2SO_4, g	0.79	0.53	0.26			0.20	0.40	0.60
ionic strength, mol/L of H_2O	0.055	0.055	0.055	0.055	0.014	0.024	0.035	0.046
limiting conv[a]	0.90	0.94	1.00	1.00	0.98	0.96	0.95	0.97
$\bar{M}_n$, 10^4	4.05	3.83	2.68	2.80	4.62	5.23	4.12	4.29
$\bar{M}_n$, 10^5	3.31	2.54	1.44	1.11	2.72	2.94	2.37	2.58
D_p by TEM, 10^3 Å	5.50	6.00	6.30	4.50	4.90	5.50	5.90	6.20
N_p by TEM, 10^{12}/cm^3 of H_2O	1.24	1.01	0.93	2.59	1.91	1.31	1.06	0.94
N_p by scattering, 10^{12}/cm^3 of H_2O	2.05	0.63	0.89	2.06	1.80	0.91	0.80	0.62
shell thickness (L), Å	114	126	240	263	225	134	261	265
av shell thickness, Å[b]				250	250			

[a] Measured at 24 h. [b] Determined from the slope of K' versus ($[KPS]^{1/2}N_p^{1/6}$) in Figure 17.

morphology were determined by use of transmission electron microscope (TEM). The particle number density (N_p) was determined by use of the mass balance and the data of $\bar{D}_p$ and conversion. The TEMs used were H-600 from Hitachi Co. and JEOL 200 CX STEM from Japan Electron Optics Laboratory. Hydrodynamic radius of the particles was measured by use of a He–Ne laser light scattering spectrophotometer (DLS-700 from Otsuka Co., Japan) for comparison. Characteristic data resulting from the measurements are also listed in Table I.

Concentration of monomer in polymer particles, $[M]_p$, was determined by the following procedure.[12] The latex samples withdrawn during the reaction were exposed to air and the monomer droplets in the latex were removed by centrifugation. The monomer-droplet-free latex was then divided into two equal parts, parts A and B. Part A was vacuum-dried after adding a hydroquinone/methanol (0.5 g/L) solution. Part B was heated to 100 °C in a closed vessel for 30 h after adding a KPS/water (1 g/L) solution and then dried. The weight fraction of polymer in the monomer-swollen particles (X_p) was determined by

$$X_p = \frac{(\text{wt of dried A})/(\text{wt of A before adding hydroquinone soln})}{(\text{wt of dried B})/(\text{wt of B before adding KPS soln})} \quad (1)$$

Assume that the volumes of monomer and polymer in monomer-swollen particles are additive, then

$$[M]_p = \frac{1 - X_p}{X_p/d_p + (1 - X_p)/d_m} \frac{1000}{W_m} \quad (2)$$

where d_m is the density of the monomer, d_p the density of the polymer, and W_m the molecular weight of the monomer.

To investigate factors that control the particle morphology and growth mechanism, we undertook seeded emulsion polymerization as follows. The seed latexes used were the final latexes of reaction runs A2, B1, and B2 as shown in Table II. Specific amounts of monomers (styrene and a minor amount of isoprene) were added to the seed latex. The reaction mixtures were agitated at 0 °C for 24 h to allow monomers to penetrate into the central region of the particles and then heated to 70 °C. Further swelling for a longer period of time did not show appreciable increase in the degree of swelling. Although the swelling was not carried out at the polymerization temperature, 70 °C, it would not affect our investigation on the presence of core–shell morphology resulting from the shell growth mechanism and on the uniform monomer distribution within the particles as discussed in the section Particle Morphology. Subsequently the initiator, KPS, was added to start the reaction at 70 °C, while for run L2 the initiator, AIBN, together with the monomers was added at the same time at the beginning of the swelling procedure. Since the residual unsaturation in the isoprene units can be stained by osmium tetroxide, the minor amount of isoprene served to tag the newly generated polymer. The recipes of the seeded emulsion polymerizations are also shown in Table II.

The ultrathin cross sections were obtained following the procedure described in the works of Williams and co-workers.[13,14] In the staining step, both aqueous and water/acetone solutions of osmium tetroxide were used. The aqueous staining was found to develop unsatisfactory contrast of the morphology. To hasten the staining efficiency, the microsections were exposed to the vapor from the mixture osmium tetroxide/water/acetone (2/49/49 wt ratio) at 25 °C for 72 h. The samples were then washed with water, vacuum-dried, and examined under the TEM.

Results and Discussion

Effect of the Hydrophilic Comonomer, AAm. The polymerizations of styrene (run A series) were carried out at various concentrations of AAm ([AAm]) with constant concentration of KPS ([KPS]) and ionic strength. $\bar{D}_p$ decreases (or N_p increases) with increasing [AAm] (Table

Table II
Recipes of Seeded Emulsion Polymerization Runs[a]

run	latex, g	St, g	KPS, g	H_2O, g	isoprene, g	AIBN, g	additives, g	D_p, μm	temp, °C	Figure
					Seed Latex					
A2		50	0.50	400			0.2 (AAm)	0.51	70	13(1), 14(1)–(4)
B1		20	0.40	400			0.4 (SLS)	0.07	70	
B2		20	0.50	400			0.4 (NaSS)	0.09	70	
					Large Emulsion Particles					
L1	50 (A2)	8	0.07	214	0.3			0.65	70	13(2)–(6)
L2	50 (A2)	4		138	0.2	0.008	0.1 (SLS)	0.55	70	16(1)–(6)
					Small Emulsion Particles					
S1	100 (B1)	40	0.30	310	0.5			0.13	65	15(1)–(2)
S2	100 (B1)	40	0.40	310	0.5			0.13	65	15(3)–(4)
S3	100 (B2)	5	0.05	181	0.1			0.11	70	15(5)–(6)

[a] St, styrene; KPS, potassium persulfate; AIBN, 2,2′-azobis(isobutyronitrile); SLS, sodium lauryl sulfate; AAm, acrylamide; NaSS, sodium *p*-styrenesulfonate; D_p, final particle diameter; temp, temperature.

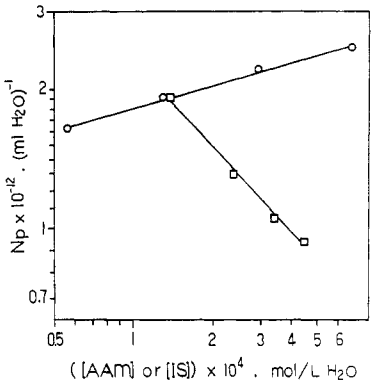

Figure 1. Logarithmic plot of particle number density, N_p, versus [AAm] for run series A (○, A2–A5) and N_p versus ionic strength (IS) for run series I (□, I1–I4).

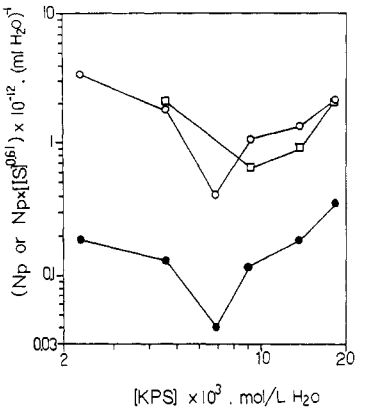

Figure 2. Logarithmic plot of particle number density, N_p, versus [KPS] without ionic strength adjustment (○, run series K, K1–K6) and the run with constant ionic strength (□, run series J, J1–J4) and the plot of $N_p[IS]^{0.61}$ versus [KPS] for run series K (●).

I). The logarithmic plot of N_p versus [AAm] is linear with the slope of 0.19 (Figure 1); i.e., N_p is proportional to $[AAm]^{0.19}$. The result is very close to that of the system using the nonionic comonomer, HEMA (0.17 power).[5]

Effect of Ionic Strength. For the run I series, the ionic strength is varied by adding various amount of the inert salt, sodium sulfate, while [KPS] and [AAm] are kept constant. In this case, $\bar{D}_p$ increases with increasing ionic strength (Table I). The logarithmic plot of N_p versus ionic strength is linear with a slope of −0.61 (Figure 1).

Effect of Initiator, KPS. Two series of experiments (series K and J in Table I) were carried out for studying effects of [KPS] on $\bar{D}_p$ and N_p. Recipes of the two series are the same except that various amounts of sodium sulfate were added to adjust the ionic strength for series J. As shown in Figure 2, each logarithmic plot of N_p verus [KPS] shows a minimum. This result is different from the linear plots in the other emulsifier-free systems (Table III). N_p is nearly proportional to the 1.29 power of [KPS] as [KPS] is within the range 7–18.5 mmol/L of H_2O.

Monomer Concentration in Monomer-Swollen Polymer Particles. Figure 3 shows weight fractions of polymer in the monomer-swollen particles, X_p, at various conversions for the systems with the lowest AAm content (A2), with the highest AAm content (A5), and without AAm (A1). As can be seen, before the disappearance of monomer droplets, the weight fraction of polymer (X_p) or the monomer concentration in the particles is constant at X_p = 0.37 and is about the same for the three systems. While after the disappearance of monomer droplets, X_p is equal to the monomer conversion, confirming that the experimental technique used in the determination of X_p is reliable. This X_p = 0.37 is equivalent to the saturated concentration of monomer in the particles, 5.8 M, which is very close to 5.5 M in the emulsifier-free system of styrene.[12] The horizontal line at X_p = 0.37 intersects the diagonal line (along which X_p equals the conversion) at the conversion 0.37, which can be regarded as the point after which the monomer droplets disappear. However, there are some deviations in the conversion range 0.27–0.42 from the theoretical curve (the horizontal line when the conversion is below 0.37 and the diagonal line when the conversion is above 0.37). Such deviations are due to the experimental difficulty in the separation of monomer droplets from the latex.

Conversion Data. The conversion curves of the A (Figure 4) and K (Figure 5) series show that the polymerization rates increase with increasing [AAm] and [KPS], respectively. All the conversion curves are concave upward until about 90% conversion, after which the curves suddenly level off and the conversions increase slowly with time. N_p versus conversion for the typical runs, A3, A5, and K1, show a constant level near 10% conversion (Figure 6), indicating that the nucleation period has ended at this conversion. Since the monomer droplets were found to disappear at 37% conversion, the particle growth period is within the conversion range 10–37%. Within this conversion range 10–37%, the log/log plot of conversion versus time gives a straight line with the slope ranging from 1.22 to 1.49 (the insets in Figures 4 and 5). Variation of the values of these slopes seems to be independent of [AAm] and [KPS]. The plot of $(\text{conversion})^{2/3}$ versus time for each of these cases also gives a straight line in the same conversion range (ca. Figure 7 for the A series). Thus, the conversion data in the particle growth period is consistent with the shell region polymerization model, which can be

Table III
Effects of Reaction Conditions on the Particle Number Density, N_p, for Some Emulsifier-Free Emulsion Polymerization Systems: $N_p \propto [\text{initiator}]^{\alpha}$; $N_p \propto [\text{comonomer}]^{\beta}$; $N_p \propto [\text{ionic strength}]^{\gamma}$

system[d]	α	β	γ	D_p, 10^3 Å	N_p, 10^{12} L/mL of H_2O	[initiator], mmol/L of H_2O	[St], mol/L of H_2O	ratio[c] × 10^3	T, °C	ref
St/KPS/H_2O	0.72		−0.71						70	11
					Nonionic Comonomer					
St/AAm/KPS/H_2O	*b*	0.19	−0.61	4.0–7.0	0.9–3.5	2.3–18.5	1.2	6.0–47	70	*a*
St/FEMA/KPS/H_2O	0.94	0.17	−0.78	5.7–7.2	1.0–2.0	3.4–11.4	2.2	2.9–23	60	5
St/AA/KPS/H_2O	0.63	0.45	−1.00	3.6–5.4	1.0–5.4	2.8–8.3	2.2	8.3–42	70	4
					Anionic Comonomer					
St/NaUI/KPS/H_2O	0.5	1.0	*b*	1.0–1.8	170–500	0.6–3.0	3.84	2.5–7.6	60	1
St/NaSS/KPS/H_2O	0.6	1.9	−1.92	1.3–5.0	3.2–65	2.8–9.0	2.4–1.0	2.0–4.0	65	30
St/NaSEM/KPS/H_2O	1.0	2.0	−0.81	1.4–9.0	0.9–250	2.8–9.0	5.2–4.1	0.4–1.8	65	30
St/NaMS/KPS/H_2O	0.3	*b*	−1.1	6.3–8.0	0.6–1.1	1.5–5.5	0.9	1.0–3.0	60	2
					Cationic Comonomer					
St/DVPM/AIBA/H_2O	1.28	*b*	−0.97	1.8–5.7	3.2–40.0	0.1–0.9	1.2–6.2	0.4–2.1	65	36
St/EMVPB/AIBA/H_2O	1.43	*b*	−1.88	2.1–5.7	3.8–45.0	0.1–0.8	2.3–4.6	0.3–0.5	65	36

[a] This work. [b] A curve with a minimum value. [c] The ratio of comonomer concentration to styrene concentration in the recipes. [d] St = styrene; KPS = potassium persulfate; AAm = acrylamide; HEMA = 2-hydroxyethyl methacrylate; AA = acrylic acid; NaUI = sodium undecylenic isethionate; NaSS = sodium styrenesulfonate; NaSEM = sodium salt of 2-sulfoethyl methacrylate; NaMS = sodium methallyl sulfonate; DVPM = 1,2-dimethyl-5-vinylpyridinium methylsulfate; EMVPB = 1-ethyl-2-methyl-5-vinylpyridinium bromide; AIBA = azobis(isobutyramidine hydrochloride).

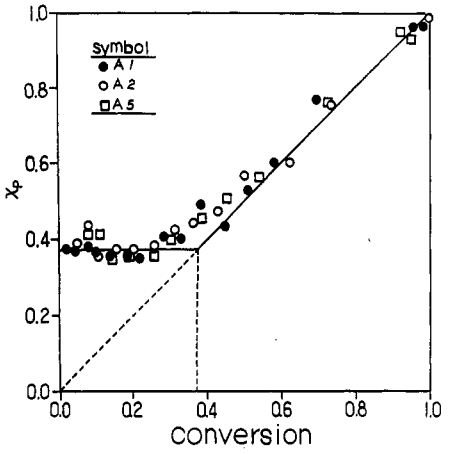

Figure 3. Weight fraction of polymer in the monomer-swollen particles, X_p, at various conversions for runs A1, A2, and A5.

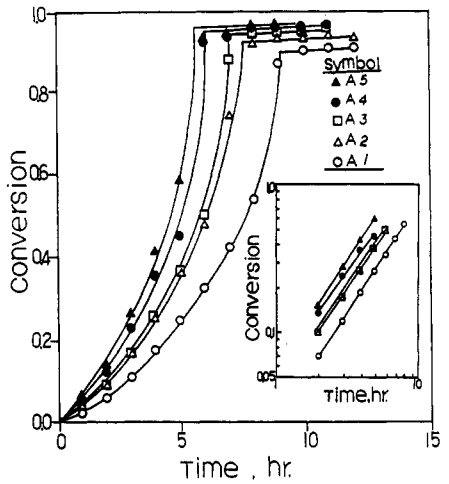

Figure 4. Conversion versus time at different [AAm] for run series A (A1–A5). The inset shows a log/log plot in which the slopes of the straight lines were determined by use of the least-square method. The slopes for A1–A5 are 1.48, 1.45, 1.46, 1.35, and 1.49, respectively.

described by the following equation:[2,3,15]

$$m^{2/3} - m_0^{2/3} = K'(t - t_0) \quad (3)$$

as was also considered by Wilkinson and co-workers[16,17] and by Chen and Chang[5] for the systems St/KPS/water and St/HEMA/KPS/water, respectively. Here m and m_0 are conversions at time t and t_0, and K' is given as

$$K' = 1.04 W_m W^{-2/3} k_{pa} [M]_s \rho_i^{1/2} N_p^{1/6} L^{1/2} / (d_p^{1/3} k_t^{1/2}) \quad (4)$$

where W_m is the molecular weight of the monomer, W the weight of the monomer in a liter of latex, $[M]_s$ the monomer concentration within the reaction loci, ρ_i the rate of initiation, L the proposed thickness of the reactive shell region in the particle, d_p the intensity of the polymer formed, and k_{pa} the apparent propagation constant. This particle growth mechanism can be termed as the "shell growth mechanism".

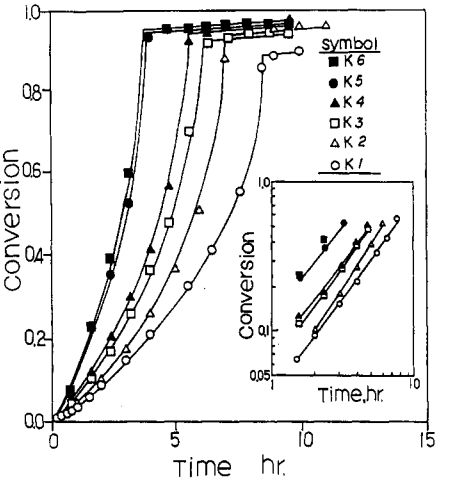

Figure 5. Conversion versus time at different [KPS] for run series K (K1–K6). The inset shows a log/log plot in which the slopes of the straight lines were determined by use of the least-square method. The slopes for K1–K5 are 1.31, 1.46, 1.36, 1.30, and 1.22, respectively. The slope for K6 was not calculated since only two data are available.

In interval II, with the assumption of constant monomer concentration in the particle, k_t is considered a constant value that is equal to $k_{t,m=0.37}$ throughout the whole interval II; while in interval III, k_t is a function of conversion as shown in Table VI. The result of the Trommsdorff effect in interval II is primarily to decrease k_t, which is a constant value, but not to accelerate the reaction rate in the whole interval II. Besides, the volume change effect was also considered in the shell reaction model as the parameter v_s, the volume of the reaction shell, in the original paper

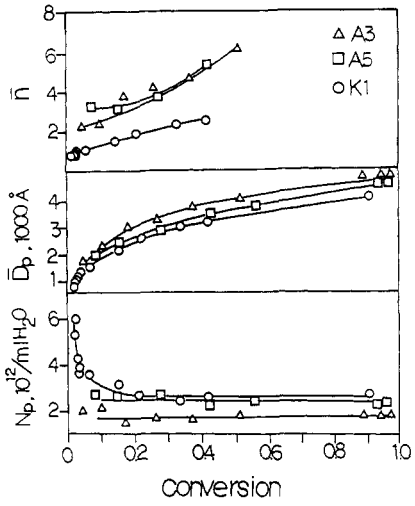

Figure 6. Variations of mean number of free radicals per particle ($\bar{n}$), particle diameter ($\bar{D}_p$), and particle number density (N_p) with conversion for runs A3, A5, and K1.

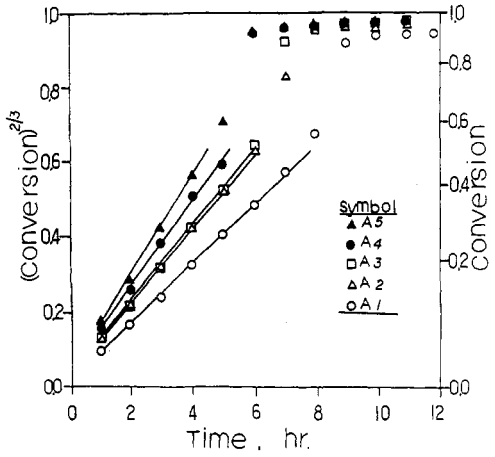

Figure 7. Plots of $(\text{conversion})^{2/3}$ versus time using the data of run series A (A1–A5) shown in Figure 4.

of Ugelstad.[15] Accordingly, the $^2/_3$ exponent of the conversion data cannot be exclusively attributed to the results of the Trommsdorff effect and the volume change effect in interval II.

In interval III ($m \geq 0.37$), the $^2/_3$ exponent of the conversion data can be extended to about 50% conversion, since the values of $([M]_s/[M]_{s,m=0.37})(k_t/k_{t,m=0.37})^{-1/2}$ are 1.00, 1.06, 1.17, and 1.31 for the conversions 0.37, 0.4, 0.45, and 0.5, respectively. According to eq 4, the observed $^2/_3$ exponent in interval III can be ascribed to the shell reaction characteristic of the present systems and to the compensation effect of the decreased rate of conversion, due to the decreased monomer concentration in the particle by the increased rate due to the increased Trommsdorff effect, as that considered by Ugelstad in the conventional emulsion polymerizations.[15]

Molecular Weight and Its Distribution. MWDs of the samples obtained after the determination of conversion for all the reaction runs are similar and those of the typical run, K1, at various conversions are shown in Figure 8. Bimodal molecular weight distributions of high polymers as well as an oligomer peak are observed in the initial period of reaction (less than about 9% conversion): the higher MW peak located at about 10^6, the medium MW peak (the major peak) at about (3×10^4)–10^5, and the oligomer peak at about 1000. The growth of the higher MW peak becomes negligible after about 10% conversion. As the polymerization proceeds further, the major peak

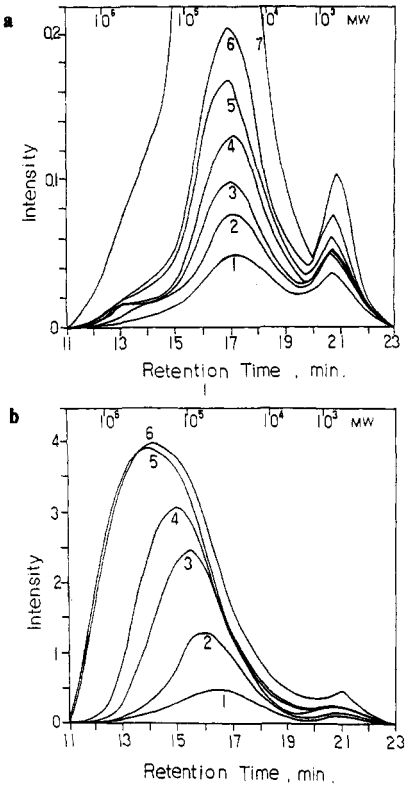

Figure 8. (a) Molecular weight distributions at different conversions of run K1: 1.2% (1); 1.8% (2); 2.1% (3); 2.7% (4); 3.3% (5); 3.9% (6); 9.3% (7). The area below each curve is about proportional to its conversion. (b) Molecular weight distributions at different conversions of run K1: 9.3% (1); 21.4% (2); 41.7% (3); 55.8% (4); 89.2% (5); 98.3% (6). The area below each curve is about porportional to its conversion.

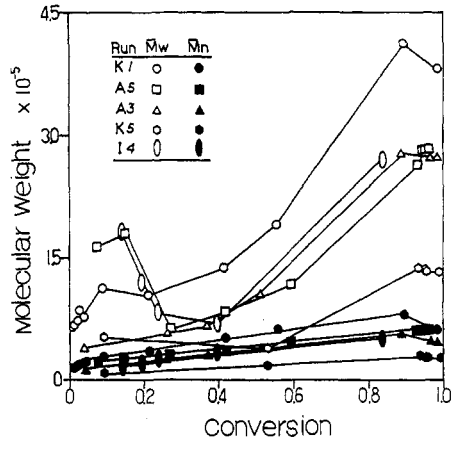

Figure 9. Variations of weight- and number-average molecular weights ($\bar{M}_w$, $\bar{M}_n$) with conversion for runs K1, A5, A3, K5, and I4. The open symbol is for $\bar{M}_w$ and the close symbol is for $\bar{M}_n$. In the determination of $\bar{M}_n$ and $\bar{M}_w$, the MW below 10^3 is omitted.

shifts gradually to the higher MW region and finally covers the higher MW peak generated in the initial period. While the oligomer peak grows continuously in the entire range of conversion, it grows more rapidly in the nucleation period. Alternatively, the growth and shift of the major peak can also be seen from the variations of the average MWs of the MWD (excluding the oligomer peak) with conversion for run K1 and some other typical runs shown in Figure 9. Only the major peak grows after about 10% conversion. This also confirms that the growing period ends at about 37% conversion, since the $\bar{M}_w$ increases steeply after this conversion. $\bar{M}_w$ increases slowly with conversion before 90% conversion and is quite different from that of the conventional case, in which $\bar{M}_n$ increases

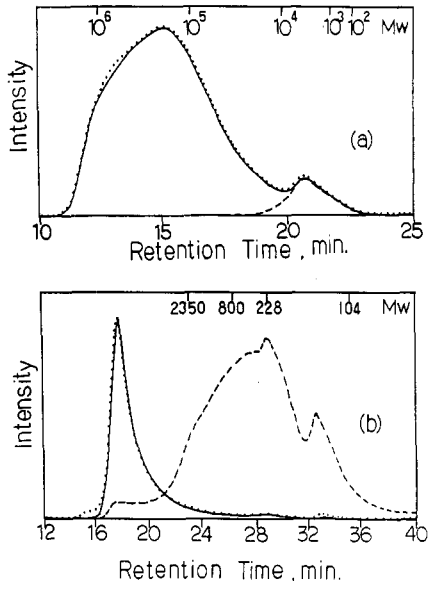

Figure 10. Molecular weight distribution of the final latex of run A1 (system styrene/KPS/H_2O) (a) using Ultrastyragel columns (Waters, exclusion limit $\bar{M}_w$ >2000) and (b) using columns A-801 and A-803 in series (Shodex, exclusion limit $\bar{M}_w$ 10–70000). (···) Latex after drying; (—) latex after replacement of the continuous phase by water four times; (- - -) polymer dissolved in the aqueous phase.

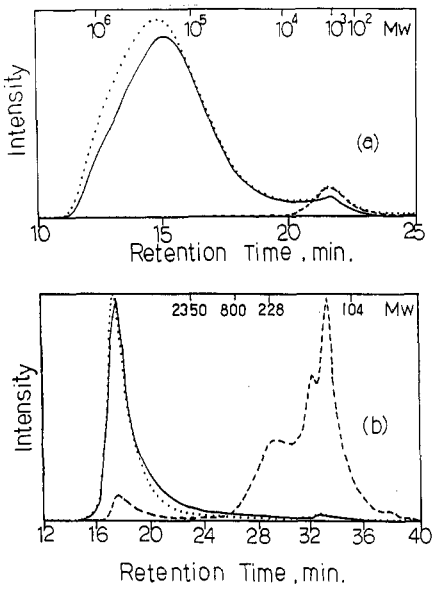

Figure 11. Molecular weight distribution of the final latex of run A5 (a) using Ultrastyragel columns (Waters, exclusion limit $\bar{M}_w$ >2000) and (b) using columns A-801 and A-803 in series (Shodex, exclusion limit $\bar{M}_w$ 10–70000). (···) Latex after drying; (—) latex after replacement of the continuous phase by water four times; (- - -) polymer dissolved in the aqueous phase.

with conversion during the particle growth period and then decreases afterward.[18,19] This would also indicate a different kinetic behavior.

The oligomer peaks as well as the bimodal MWD of high polymers in Figure 8a were also found in the system St/KPS/water.[9] However, by use of GPC columns with the exclusion limits from 10 to 7 × 10^4, the oligomer peak becomes a broad distribution having MWs in the range 200 to a few thousands (Figures 10 and 11). A majority of the oligomers have MWs in the range 200–800. Note that the samples involve polymers in the particles and in the aqueous phase. In order to clarify the origin of the oligomer peak, the final latexes of runs A1 and A5 were subject to the following treatment for separating polymers in the particle and aqueous phase. By centrifugation, the particles in the latex were precipitated. The clear solution above the precipitate was removed, filtrated through a filter with an average pore size of 0.2 μm, and then dried under vacuum. The polymers (and oligomers) in the particle phase (the precipitate) and in the aqueous phase were both subject to MWD measurements. The results are shown in Figures 10 and 11. For the systems St/KPS/H_2O (run A1) and St/AAm/KPS/H_2O (run A5), not all the oligomers were adsorbed on the polymer particles, but a considerably large part (about 14–40 wt % as shown in Table IV) was dissolved in the aqueous phase.

Particle Morphology. TEM micrographs of the polymer particles at various conversions of the typical run (K1) are shown in Figure 12. The particles at the earlier stage (at 1.76% conversion) have the morphology of a sphere with an empty core (Figure 12(1)), as the latex on the copper grid was dried under dynamic vacuum. This morphology was also found in the systems St/KPS/water.[9] While the latex dried in a quiescent desiccator, the particles have solid sphere morphology. These observations would indicate that the particles have a uniform monomer distribution even though polymerization might occurs only in the shell region. The empty core morphology resulted from a flash evaporation of the styrene in the small particles (of which the surface to volume ratio is so high, allowing a high mass transfer rate per unit surface area) during the dynamic vacuum pumping.

At 9.3% conversion, the particles show an anomalous shape (Figure 12(2)), as that in the system St/HEMA/KPS/water.[5] This indicates that the particles in the earlier stage involve polymerization of a significant amount of AAm units in the surface region, allowing the absorption of a considerable amount of water. Thus during drying the latex on the copper grid for TEM observation, the particles exhibit an anomalous shape with an uneven surface. When the polymerization proceeds further at 33.3% and 90.3% conversions, the particles became spherical as shown in parts 3 and 4 of Figures 12, respectively. This is due to lowering of the AAm units relative to the styrene units in the particles.

Figures 13–16 show the electron micrographs of some sectioned particles obtained from the seeded emulsion polymerizations with different sizes of the seed particles (Table II). The sectioned particles are highly distorted and are larger than the original particles. This is due to a high shear stress produced during microtome sectioning and to a swelling of the particles by absorption of the embedding resin during the sample preparation, respectively. Nevertheless, the contrast of the electron micrographs still develops so well as that the characteristic morphology of the present systems can be easily identified in Figures 13–16. It is also obvious that each particle is spherical and has uniform size before and after the polymerization process as shown in Figures 13–16. Thus each particle was subject to the same extent of reaction, and the electron micrograph of any sectioned particle is representative.

Figure 13 shows the electron micrographs of some sectioned particles obtained from the seeded emulsion polymerization with the final latex of run A2 as the seed, which has the diameter of 5100 Å. The composition of the reaction mixture L1, (the final latex of A2)/St/isoprene/KPS/H_2O, is 50/8/0.3/0.07/214 by weight. A comparison of parts 3 and 4 of Figure 13 for the unstained and stained sectioned particles of run L1, respectively, shows that only the shell region of the particle was stained; i.e., polymerization only occurred in this region. By partial replace-

Table IV
Weight Fractions of the Polymer Composition Calculated from Figures 10 and 11

sample	system	wt % of oligomers rel to total polymers	wt % of high polymers washed away rel to total polymers	wt % of oligomers washed away rel to total polymers	wt % of oligomers washed away rel to total oligomers
A1	St/KPS/H_2O	7%		1%	14%
A5	St/AAm/St/H_2O	5%	10%	2%	40%

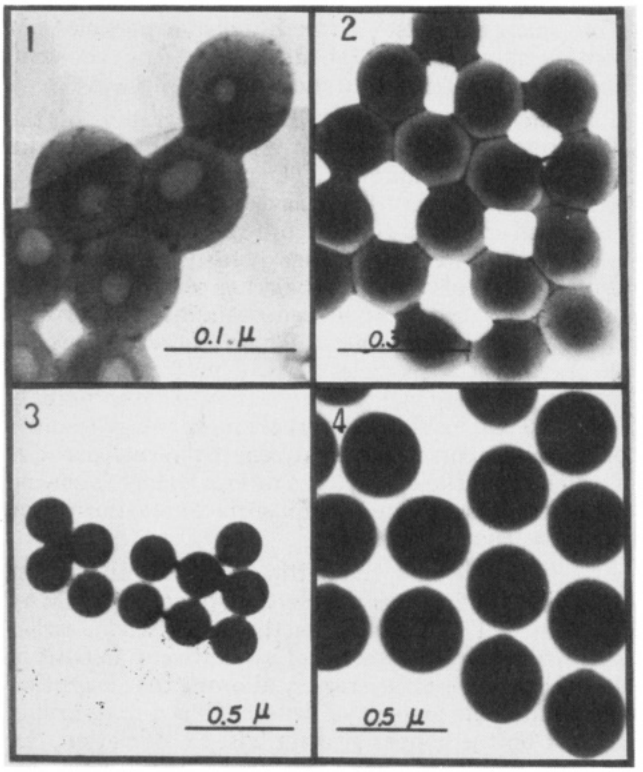

Figure 12. TEM micrographs of polymer particles at different stages of polymerization for run K1: (1) 20 min, 1.76% conversion; (2) 2 h, 9.3% conversion; (3) 5.5 h, 33.3% conversion; (4) 10 h, 90.3% conversion.

ment of water with acetone in the OsO_4 solution for staining, the dark–white contrast is much sharper (Figure 13(5),(6)).

The dark ring in Figure 13(4)–(6) cannot be due to phase separation of polystyrene and styrene–isoprene copolymer within the particle, because the dark region in the micrograph of stained film cast from toluene solution (Figure 14(1),(2)) is quite different from those of the core–shell morphology shown in Figure 13(5),(6). It cannot also be due to higher acrylamide content in the region close to the surface, since the micrograph of the OsO_4-stained sectioned seed particle shows no dark ring (Figure 14-(3),(4)).

In order to further explore the particle growth mechanism, D_p of the seed is reduced to 0.07 and 0.09 μm (obtained from runs B1 and B2); particles of the resulting latexes S1, S2, and S3 have D_p of 0.13, 0.13, and 0.11 μm, respectively. Their microtome-sectioned particles exhibit uniform morphology as shown in Figure 15(2),(4),(6), indicating that polymerization occurred uniformly within the small particles. Thus the core–shell morphology in Figure 13 and the homogeneous morphology in Figure 15 provide strong evidence for the occurrence of the shell growth mechanism in the large emulsion particles but not in the small particles.

To elucidate the dominating factor for the formation of the core–shell morphology, we also used the oil-soluble initiator, AIBN, instead of the water-soluble initiator, KPS,

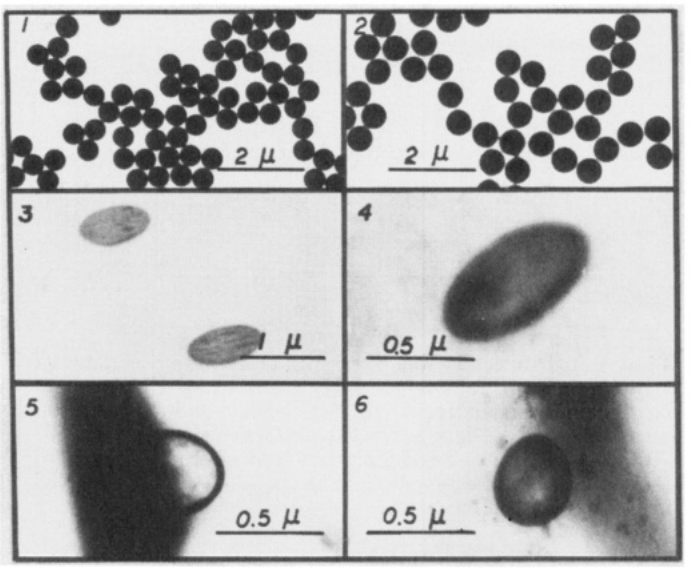

Figure 13. Transmission electron micrographs of the core–shell morphology, OsO_4 stained: (1) particles of the seed A2; (2) particles of L1; (3–6) microtome sections of particles of L1; (3) unstained; (4) stained by aqueous OsO_4 solution for 2 weeks; (5, 6) stained by vapor of the solution OsO_4/acetone/water for 3 days.

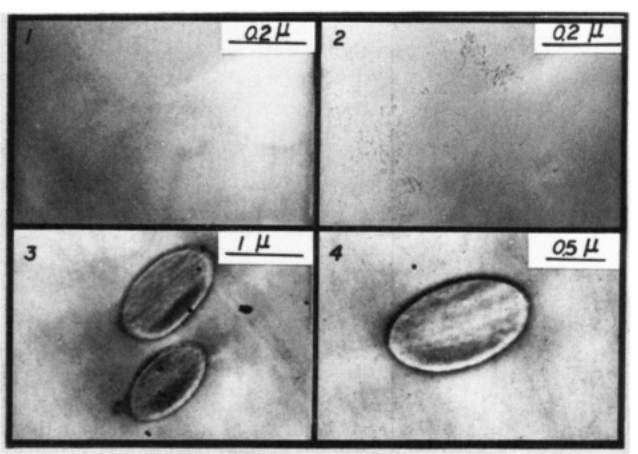

Figure 14. Transmission electron micrographs of run A2, OsO_4 stained: (1, 2) solution-cast film; (3, 4) microtome sections of the particles.

in reaction run L2. As monomer is distributed everywhere in its seed, the introduction of the oil-soluble initiator, AIBN, should allow styrene to react with isoprene everywhere within the particle. The microtome-sectioned particles of L2 show uniform morphology as shown in Figure 16(2)–(6). The observation further indicates that the core–shell morphology should not be due to nonuniform swelling or a monomer diffusion-controlled mechanism. In addition, this observation also indicates that swelling for 24 h is enough for the monomers to diffuse into the center of each emulsion particle.

Although the degree of swelling at 0 °C could be different from that at 70 °C and monomer distribution in the particles during the polymerization at 70 °C may not be

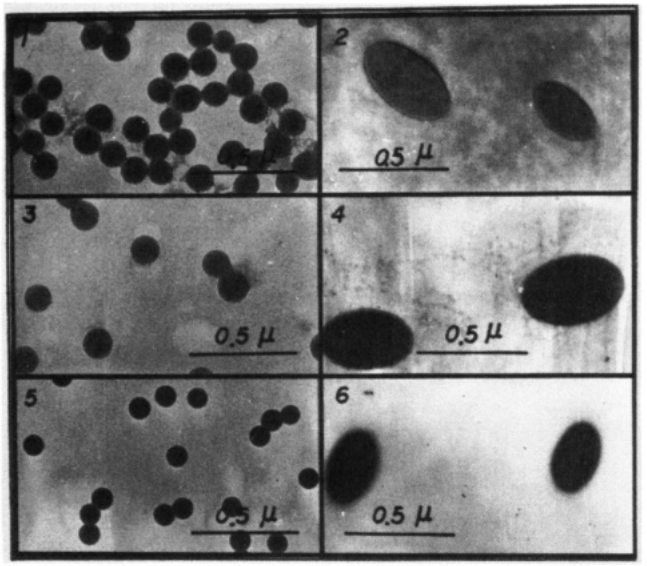

Figure 15. Transmission electron micrographs of the homogeneous morphology for small particles, OsO_4 stained: (1) particles of run S1; (2) microtome sections for particles of run S1; (3) particles of run S2; (4) microtome sections for particles of run S2; (5) particles of run S3; (6) microtome sections for particles of run S3.

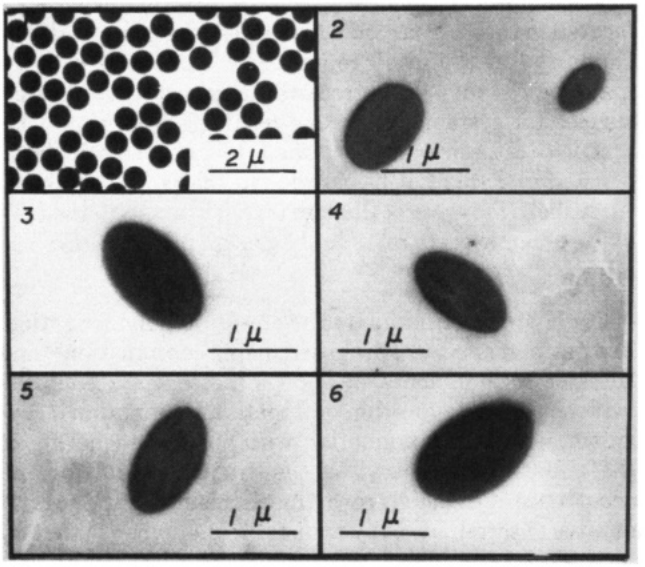

Figure 16. Transmission electron micrographs of the homogeneous morphology with oil-soluble initiator, AIBN, OsO_4 stained: (1) particles of run L2; (2–6) microtome sections for particles of run L2.

in an equilibrium state, the presence of homogeneous morphology for the cases of the large seed (0.51 μm) with AIBN and small seeds (0.07 and 0.13 μm) with KPS as initiators as discussed in the above paragraph indicates that monomer did distributed everywhere in the particles if treated in accordance with the swelling procedure at 0 °C. Thus if the latex particles are allowed to swell at 70 °C until an equilibrium state is reached, the same result of homogeneous morphology should be expected. The reasons why we did not allow the particles to swell at 70 °C are that parts of the styrene could polymerize via a thermal polymerization mechanism and that a high percentage of the minor amount of added isoprene monomer might evaporate during the swelling, since its boiling point is only 34.1 °C. Thus, for the presence of the core–shell morphology in run L1, swelling at 0 °C should give the same result as that at 70 °C.

Table V
Estimated Initial Instantaneous Copolymer Composition in the Aqueous Phase

run	A2	A3	A4	A5
[AAm], (L of H_2O)$^{-1}$	0.007	0.014	0.028	0.056
[St], (L of H_2O)$^{-1}$	0.003	0.003	0.003	0.003
F_{AAm}[a]	0.512	0.647	0.767	0.860

[a] F_{AAm} is the molar ratio of AAm units of the polymer generated in the aqueous phase as calculated from $F_1 = (r_1f_1^2 + f_1f_2)/(r_1f_1^2 + 2f_1f_2 + r_2f_2^2)$ and $F_2 = 1 - F_1$. The reactivity ratios used are $r_1 = 1.44$ and $r_2 = 0.30$ in the polar solvent, ethanol,[34] where 1 and 2 refer to styrene and acrylamide, respectively.

The core–shell morphology for polystyrene emulsion particles has been observed long ago by Williams and co-workers.[13,14] They attributed this occurrence to a thermodynamic factor such that, in the particle growth period, each particle consists of a polymer-rich core with relative little monomer and a monomer-rich shell. However, no sufficient evidence was given to support their interpretation.[15,20,21] Besides, the emulsion particles prepared by Williams et al. were synthesized by using the nonionic surfactant Triton-X-100 (octylphenoxyethylene oxide), which can create a strong chain-transfer reaction and may mislead the experimental observations.[15]

Particle Nucleation Mechanism. Recall the observations that about 40% of the total oligomers is soluble in water (Table IV) in the final latex of run A5 and that, resulting from the TEM result (Figure 12(2)), a significant amount of AAm units relative to styrene units is located in the surface region when conversion is less than 9.3%. These two observations would favor an occurrence of the homogeneous nucleation mechanism as described below. In the beginning of the polymerization, KPS is thermally decomposed into primary radicals to induce the copolymerization of styrene and AAm in the aqueous phase. The so-formed copolymers or their radicals could either be soluble in the aqueous phase or coagulate to form primary particles, depending on their AAm content and MW. This coagulative nucleation mechanism has been proposed by Napper and co-workers[10] for emulsifier-free emulsion polymerization. During the nucleation period, the AAm content in the polymer chains in the particles is rather high as calculated from the copolymer composition equation (Table V). Most of the AAm-rich chains would preferably locate on the particle surface. As collision between the primary particles occurs, particle coagulation could take place due to insufficient surface charges and mutual entanglements of chains on the surface of the colliding particles. After the particle coagulation, more stable particles would form due to an increase of surface charge density. Due to the coagulation, the stable particles would have uniform size and large diameter, about 2000 Å at end of the nucleation period, and have N_p less than those in systems with the ionic comonomers (Table III). As polymerization proceeds further, more ionic groups from the decomposition of KPS could be incorporated on the particle surface to provide more electrostatic repulsive forces, and the polymers in the particles will contain more styrene units to harden the particles. Both factors will cause the particles to become more stable.

Recall that N_p is proportional to the 0.19 power of [AAm], to the −0.61 power of [ionic strength], and to the 1.29 power of [KPS] (as [KPS] is within the range of 7–18.5 mmol/L of H_2O). Obviously, among these reaction parameters, [KPS] plays a predominant role in the particle nucleation period. The 0.19 power of [AAm] is much less than that of the [anionic comonomer], which is about 1.0–2.0, as shown in Table III. This observation implies that

Table VI
Kinetic Constants and Characteristic Data for the Systems St (M1)/AAm (M2)

parameters	values	temp, °C	solvent	ref
k_d of KPS	2.7×10^{-5} s^{-1}	70	water	17
k_{p11}	480 (L/mol·s)	70		23
k_{p22}	6×10^3 L/mol·s	25	water, pH 5.5	35
k_{t11}, $(k_{t0})^a$	6.1×10^7 L/mol·s	70		23
k_{t22}	3.3×10^6 L/mol·s	25	water, pH 5.5	35
$k_{p11}/(k_{t11})^{1/2}$	0.06 (L/mol·s)$^{1/2}$			
$k_{p22}/(k_{t22})^{1/2}$	3.3 (L/mol·s)$^{1/2}$			
$(k_{tr,M})_{St}$	1.9×10^{-2} L/mol·s	70		37
$(k_t)_{St}$[b]	$k_{t0} \exp[-2(Bm + Cm^2 + Dm^3)]$			37
	conversion, $m > 0.27$			
	$B = (2.57 - 5.05) \times 10^{-3}T$			
	$C = (9.56 - 1.76) \times 10^{-2}T$			
	$D\ (-3.03 + 7.85) \times 10^{-3}T$			
reactivity ratios	$r_1 = k_{11}/k_{12}$, $r_2 = k_{22}/k_{21}$			
	$r_1 = 1.44 \pm 0.22$, $r_2 = 0.30 \pm 0.09$	70	ethanol	34
	$r_1 = 0.25$, $r_2 = 12.5$		benzene	33
partition coeff	[AAm] in St/[AAm] in H_2O = 0.093			6
solubility	215.5 g of AAm/100 g of H_2O	30		
	0.032 g of St/100 g of H_2O	room temp		38
MW of monomer	St, 104.14; AAm, 71.08			
density, g/cm^3	St, 0.906; AAm, 1.122; polystyrene, 1.065			

[a] Extrapolated from 50 °C and 60 °C data of k_{t0} by assuming an Arrhenius form of k_{t0}. [b] $k_t = 1.3 \times 10^7$ L/mol·s is used in the calculation of $\bar{n}$ and L before the disappearance of monomer droplets ($m = 0.37$).

the effect of [AAm] on N_p is much less than that of anionic comonomers. This consideration can also be supported by the fact that N_p in the present system is about 10^{12} per mL of water, about 1–2 orders lower than those of systems using the anionic comonomers.

The existence of a minimum N_p as [KPS] varies indicates a competition between the nucleation and particle coagulation, as revealed below. Since the pH value of the aqueous phase is about 4.0 due to the presence of KPS, the protons (H^+) can be incorporated with the amide groups on the AAm units to form protonated amide ions carrying positive charge. The positive charges can then interact with the sulfate groups (OSO_3^-) on the chain ends, causing a reduction of the electrostatic repulsive forces among the particles. As [KPS] increases, the increase in the number of precipitated chains cannot compensate for the increased coagulation. Thus N_p decreases as [KPS] increases at lower [KPS] (Figure 2). As [KPS] is higher than 7 mmol/L of H_2O, N_p increases with [KPS] and is about proportional to [KPS]$^{1.29}$. This is due to that the rate of generation of precipitated chains is so high, allowing an over-compensation for the increased coagulation.

The Particle Growth Mechanism in the Postnucleation Period. All the conversion curves in the present St/AAm systems are concave upward. The log/log plots of conversion versus time have the slopes ranging from 1.22 to 1.49 during the particle growth period (the insets of Figures 4 and 5). From a theoretical standpoint, for the "Smith–Ewart case III", the slope is 2, while for the "Smith–Ewart case III applied to the shell reaction model" it is 1.5.[3,15,22] Accordingly, the experimental results are more consistent with the Smith–Ewart case III applied to the shell reaction model, and the particle growth mechanism is termed the shell growth mechanism.

According to eq 4, the shell thickness, L, can be calculated. k_{pa} in the equation could vary with monomer composition, which is also changing as the reaction proceeds. However, no datum of k_{pa} for the present system is available. Fortunately, for the present St/AAm system, k_{pa} can be taken as k_p of styrene (480 L/mol·s)[23] as shown in the Appendix.

Note that the shell with a thickness L is a moving layer during the growth period within which the reaction occurs. The occurrence of the shell reaction indicates a presence of propagating polymer radicals with the sulfate end groups anchored on the particle surface and the growing ends located in the shell region. This consideration can also be supported by the result reported by Vanderhoff[24] that a major part of the sulfate groups are exposed on the particle surface for systems of styrene resulting from conductometric titration works. The shell thickness so calculated is listed in Table I; it has a value in the range ~100–400 Å. A shell thickness of this size is consistent with the MW of the polymers generated in the growth period as revealed later.

For chain termination in the emulsion polymerization, two mechanisms were proposed, being combination[24] and transfer to monomers.[25] For the present systems, the evidence below favors the combination termination mechanism, which, in conjunction with surface anchoring of the sulfate end groups, is the "requirement" for the occurrence of the shell growth mechanism. First, the ratio of rates of termination by transfer to monomer to that by bimolecular combination $(k_{tr,M}[M]_p/(k_{tc}[R])$ can be estimated as $(2.6 \times 10^{-3}–(1.3 \times 10^{-2})$. Here $k_{tr,M}$ and k_{tc} are rate constants for transfer to monomer and combination, respectively, and are listed in Table VI. The particle diameter is taken as 5000 Å, $\bar{n}$ as 10–2, and $[M]_p$ as 5.8 M. This result shows that chain termination by transfer to monomer is negligible. Second, the result of end-group titration given by Vanderhoff[24] shows that each chain was formed through radical combination. Third, if chain transfer to monomer should occur, the core–shell morphology would not develop. However, in the present system, the core–shell morphology obviously exists for particles with a seed diameter of 5100 Å.

The plots of K' versus $[KPS]^{1/2}N_p^{1/6}$ are linear for series A, K, and J in Figure 17. The straight line passing through the origin for series K (varying [KPS]) indicates a constant shell thickness (about 250 Å). While for series J and A (varying [KPS] at constant ionic strength and [AAm], respectively), the straight lines do not pass through the origin, indicating that the shell thickness (L) varies with [AAm] or ionic strength.

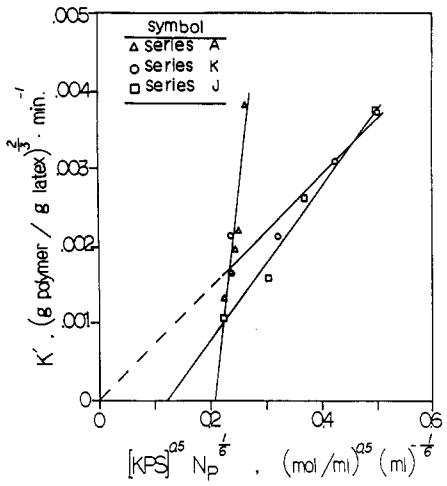

Figure 17. Plots of the slopes of K' versus $[KPS]^{1/2}N_p^{1/6}$ of the linear portions in Figure 7 (series A) and those of series K and J.

It is informative to know the average number of free radicals per particle ($\bar{n}$), which can be calculated by

$$r_p = k_{pa}[M]_p\bar{n}/Na \quad (5)$$

where r_p is the rate of polymerization per particle, k_{pa} the apparent rate propagation constant, $[M]_p$ the total monomer concentrations in a particle at time t, and Na the Avogadro number. Before disappearance of monomer droplets, the particles are saturated with monomers as in the conventional case, and $[M]_p$ can be taken as 5.8 M (equivalent to 37% conversion after which the monomer droplets disappear). Since the concentration of AAm in the particle phase is so small, the apparent k_{pa}, which is estimated to be 480.4 L/mol·s, can be taken as k_p in the systems of pure styrene (480 L/mol·s) as shown in the Appendix. Using eq 5 and calculated r_p from the conversion data, $\bar{n}$ value versus conversion for runs A4, A5, and K1 were calculated as shown in Figure 6. It shows that $\bar{n}$ increases with conversion and reaches the values of about 2–6 at about 40% conversion, much higher than that of the conventional case.

The MWD measurements are also consistent with the shell growth mechanism, as revealed below. The bimodal MWD of high polymers in the nucleation period implies that there are two kinds of reaction loci in the particles. Besides, for polystyrene at Θ condition,[26] the root-mean-square end-to-end distance $(\langle \bar{r}^2 \rangle)^{1/2}$, calculated from the equation $(\langle \bar{r}^2 \rangle/M_w)^{1/2} = 0.71$ Å, is 710 Å for $\bar{M}_w = 10^6$ and 225 Å for $\bar{M}_w = 10^5$. The former MW is typical for the conventional case[27] (Smith–Ewart case II) and for the earlier stage of the nucleation period in the present St/AAm system; while the latter MW is typical in the shell growth period. Such low MW in the growth period must be due to the growing radicals having a greater chance to terminate with the other entering radicals or the growing radicals in the reactive region of the particle.

From the analysis above, it is clear that the shell growth mechanism is well consistent with the conversion and MWD data. The TEM examination in Figure 13 for the seeded emulsion polymerization of styrene, with trace amount of isoprene to serve as a tag for the newly generated polymer, also gives strong evidence for the existence of the reaction shell. This reaction shell solely resulted from the large particle size and surface anchoring of the sulfate ends of the growing radicals.

As polymerization proceeds to the conversions above 10%, the lower MW (about (3×10^4)–10^5) mode gradually shifts to the higher MW region and covers the higher MW

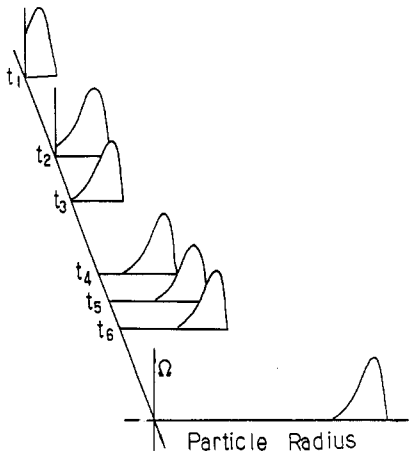

Figure 18. End-to-end distance distribution function (Ω) of a radical chain in the particle at different reaction times.

(10^6) mode generated in the initial period (Figure 8b). The 10^6 peak is contributed from polymerization in the particle rather than from copolymerization of styrene with acrylamide in the aqueous phase as revealed in the Appendix. The increase of the number-average molecular weight ($\bar{M}_n$) with conversion in Figure 9 can be illustrated by use of the end-to-end distance distribution of the growing radicals in the particles (Figure 18).[28] In the particle, the growing end of the radical would be removed from its hydrophilic end (which is anchored on the particle surface) by the most probable end-to-end distance. Of course, there is some chance, though small, that the end-to-end distance could be higher than the most probable value. As the shell growth mechanism occurs, the radical ends located outside the shell region having a thickness equal to the most probable end-to-end distance would have less chance to be terminated. Thus, as the particle grows larger, the average MW of the newly generated polymer would increase slowly with conversion before 37% conversion is reached. After this conversion, the MW increases rapidly due to the strong gel effect in the particles.

As the reaction proceeds to about 90%, the conversion curve levels off due to lack of monomer, and the monomer diffusion controls the reaction. Thus, the MWD shifts slightly toward the lower MW side in this period (Figure 8b). This observation of MWD was not found in the systems St/KPS/water in our laboratory. The reason for this difference is probably that, for the present system, the polymer chains exposed on the particle surface have additional nonionic hydrophilic units (acrylamide), causing the packing of the sulfate groups (OSO_3^-) on the particle surface to be looser. This allows the oligomeric radicals generated in the water phase to be absorbed more easily into the particles to take part in the polymerization.

According to the description above, the occurrence of the reaction shell is due to the large particle size and surface anchoring. Thus, one might expect that this mechanism could also occur in the conventional case, having sufficient particle size. Hasan's[29] result on the seeded emulsion polymerization of styrene with the presence of emulsifier shows that this is the case. As the diameter of the seed latexes is less than about 1200 Å (e.g., 660, 860, and 1140 Å), there is a constant rate period up to 50% conversion. As the diameters of the seed particles are greater than about 2000 Å (e.g., 2030, 3370 Å), the conversion curves before the disappearance of monomer droplets are concave upward, as are those in the present St/AAm systems. Our calculation on his conversion data again shows that values of the slopes in the log/log plots of conversion versus time

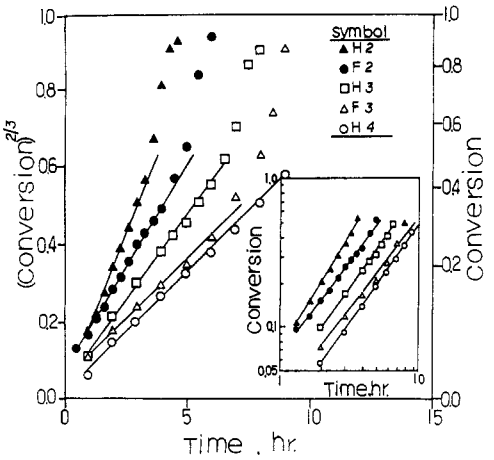

Figure 19. Plots of (conversion)$^{2/3}$ versus time of Hasan's[29] data for various seeding experiments. The diameter of the seed is 2030 Å for each run except for run F3 (3370 Å). The inset shows a log/log plot in which the slopes of the straight lines for H2, F2, H3, F3, and H4 are 1.52, 1.26, 1.33, 1.23, and 1.35, respectively.

range from 1.23 to 1.52 (Figure 19), close to "1.5" for the shell growth mechanism.

On the other hand, emulsifier-free systems with ionic comonomers can sometimes give a period of constant polymerization rate in the particle growth period as in the conventional case when its particle size is small, such as the systems with sodium undecylenic isethionate (NaUI)[1] and sodium styrene sulfonate (NaSS)[30] as comonomers, in which the final particle diameters range from 1080 to 1820 Å and 1480 to 2020 Å, respectively. The values of $\bar{n}$ calculated from the original data of the former system by using eq 5 are about 0.40, further confirming that the particle growth behavior follows the Smith–Ewart case II.

All the results discussed above indicate that the occurrence of the shell region polymerization is solely due to the large size of the particles. The reason this is usually observed in the emulsifier-free systems is due to the lack of charge density on the particle surface in the nucleation period, which results in serious coagulation of the primary particles and therefore in the formation of large particles.

Conclusion

Particle nucleation is likely via the homogeneous nucleation mechanism. During the nucleation period, particle coagulation also occurs. The particle grows in accordance with the shell growth mechanism, as the particle has a diameter greater than about 1500–2000 Å, by which the reaction only occurs in the shell region, having a shell thickness of about 100–400 Å. Monomer distribution in the particle is considered to be uniform in the entire growth period.

Acknowledgment. We thank the National Science Council for financial aid through the project Studies on Emulsion Polymer Systems, NSC 79-0405-E007-05.

Appendix: Effects of [AAm] on k_{pa} and MWD

For copolymerization systems, the overall rate of polymerization can be expressed in terms of the apparent rate constant as

$$R_p = -dM/dt = k_{pa}X_T M \qquad \text{(A-1)}$$

as proposed by Kuo and Chen[31] and by us,[32] where k_{pa} denotes the apparent rate constant of propagation. M refers to the total concentration of monomers A and B in the reaction mixture at reaction time t, and X_T represents the concentration of the two types of polymeric radicals in the reaction mixture at time t. In this treatment, k_{pa} is defined as[31]

$$k_{pa} = \frac{(k_{12}k_{21} - k_{11}k_{22})f_1 f_2}{(k_{21} - k_{11})F_2 f_1 + (k_{12} - k_{22})F_1 f_2} \qquad \text{(A-2)}$$

where k_{ij} refers to the rate propagation constant of radical species i to monomer species j. F_i and f_i are the polymer and monomer compositions for the chemical species i.

For the systems St/AAm, no data of k_{pij} in water and in styrene are available. Estimation of the rate constants is necessary in order to determine the effects of [AAm] on the apparent rate constants and MWD. Acrylamide monomer has little tendency to copolymerize with styrene in nonpolar medium.[33] On the other hand, when acrylamide monomer is highly hydrogen bridged or strongly affected by dipolar interactions, styrene has little tendency to copolymerize with acrylamide. Thus the reactivity ratios in the polar solvent, ethanol,[34] and in the nonpolar solvent, benzene,[33] can be adopted as the approximated values in water and styrene, respectively. The kinetic constants and the partition coefficients used for the calculation are shown in Table VI.

For acrylamide in water, the value of k_{p22}, 6×10^3 L/mol·s, and that of $k_{p22}/(k_{t22})^{1/2}$, 3.3 (L/mol·s)$^{1/2}$, are extremely large in comparison to those of styrene, 480 L/mol·s and 6.0×10^{-2} (L/mol·s)$^{1/2}$, respectively.[23,35] As a result, the acrylamide could polymerize to give polymers with molecular weights in the millions. However, the reactivity ratios of St(M1) and AAm(M2) in the polar solvent, ethanol, are $r_1 = 1.44$ and $r_2 = 0.3$,[34] which mean that, in a polar solvent, acrylamide radicals are readily converted to styrene radicals even at low styrene concentrations because of the high reactivity of both acrylamide radicals and styrene monomers. The estimated k_{pa} in water is 1000 L/mol·s, which is lower than that of AAm alone by a factor of about 6 and is higher than that of St alone by a factor of about 2, while the k_{ta} can be approximated as k_{t11} listed in Table VI. Since the kinetic chain length is proportional to $k_p/(k_t)^{1/2}$, the estimated MW of the copolymer generated in the aqueous phase is on the order of 10^4. Thus, the molecular weights of St/AAm copolymers in the aqueous phase are expected to be much lower than those with acrylamide alone. In addition, the bimodal MWD of high polymers was also observed in the emulsifier-free systems of pure styrene.[9,16] Therefore, the higher MW peak (MW = 10^6) in the early stage of the reaction must come from polymerization in the small particles, which follows the Smith–Ewart case II theory, and not from the copolymerization of AAm and styrene in the aqueous phase.

In the particle phase, though, k_{pa} can be strongly affected by the comonomer composition in the feed and composition shift during the reaction as shown in eq A-2. Nevertheless, in our experiments, the concentration of AAm in the particle phase is so small ($f_2 \cong 1.2 \times 10^{-3}$) that AAm can hardly increase the value of k_{pa}. The calculated value of k_{pa} is 480.4 L/mol·s, which is very close to that in the systems of pure styrene, 480 L/mol·s.[23] This result can also be supported by another independent experimental result for the St/AAm system; namely, after particle formation, styrene polymerized exclusively in the particles until styrene droplets disappeared.[6] Therefore, the propagation rate constant of pure styrene can be applied to the postnucleation period in the estimation of $\bar{n}$ and the shell thickness of the growing particles for the emulsion copolymerization systems of St/AAm.

References and Notes

(1) Chen, S.-A.; Chang, H.-S. *J. Polym. Sci., Polym. Chem. Ed.* **1985**, *23*, 2615.
(2) Chang, H.-S.; Chen, S.-A. *J. Polym. Sci., Polym. Chem. Ed.* **1988**, *26*, 1207.
(3) Chang, H.-S.; Chen, S.-A. *Makromol. Chem., Rapid Commun.* **1987**, *8*, 297.
(4) Chen, S.-A.; Lee, S.-T.; Lee, S.-J. *Makromol. Chem., Macromol. Symp.* **1990**, *35/36*, 349.
(5) Chen, S.-A.; Chang, H.-S. *J. Polym. Sci., Polym. Chem. Ed.* **1990**, *28*, 2547.
(6) Ohtsuka, Y.; Kawaguchi, H.; Sugi, Y. *J. Appl. Polym. Sci.* **1981**, *26*, 1637.
(7) Tamai, H.; Murakami, T.; Suzawa, T. *J. Appl. Polym. Sci.* **1985**, *30*, 3857.
(8) Ceska, G. W. *J. Appl. Polym. Sci.* **1974**, *18*, 427, 2493.
(9) Goodall, A. R.; Wilkinson, M. C.; Hearn, J. *J. Polym. Sci., Polym. Chem. Ed.* **1977**, *15*, 2193.
(10) Feeney, P. J.; Napper, D. H.; Gilbert, R. G. *Macromolecules* **1987**, *20*, 2922.
(11) Goodwin, J. W.; Hearn, J.; Ho, C. C.; Ottewill, R. H. *Br. Polym. J.* **1973**, *5*, 347.
(12) Chiu, W.-Y.; Shih, C.-C. *J. Appl. Polym. Sci.* **1986**, *31*, 2117.
(13) Grancio, M. R.; Williams, D. J. *J. Polym. Sci., Part A-1* **1970**, *8*, 2617.
(14) Keusch, P.; Williams, D. J. *J. Polym. Sci., Polym. Chem. Ed.* **1973**, *11*, 143.
(15) Ugelstad, J.; Hansen, F. K. *Rubber Chem. Technol.* **1976**, *49*, 536.
(16) Hearn, J.; Wilkinson, M. C.; Goodall, A. R.; Chainey, M. *J. Polym. Sci., Polym. Chem. Ed.* **1985**, *23*, 1869.
(17) Chainey, M.; Hearn, J.; Wilkinson, M. C. *J. Polym. Sci., Polym. Chem. Ed.* **1987**, *25*, 505.
(18) Grancio, M. R.; Williams, D. J. *J. Polym. Sci., Part A-1* **1970**, *8*, 2733.
(19) Lin, C.-C.; Chiu, W.-Y. *J. Appl. Polym. Sci.* **1979**, *23*, 2049.
(20) Gardon, J. L. *J. Polym. Sci.* **1973**, *11*, 241; **1974**, *12*, 2133.
(21) Napper, D. H. *J. Polym. Sci., Part A-1* **1971**, *9*, 2089.
(22) Smith, W. V.; Ewart, R. H. *J. Chem. Phys.* **1948**, *16*, 592.
(23) Buback, M.; Garcia-Rubio, L. H.; Gilbert, R. G.; Napper, D. H.; Guillot, J.; Hamielec, A. E.; Hill, D.; O'Driscoll, K. F.; Olaj, O. F.; Shen, J.; Solomon, D.; Moad, G.; Stickler, M.; Tirrell, M.; Winnik, M. A. *J. Polym. Sci., Polym. Lett.* **1988**, *26*, 293.
(24) Vanderhoff, J. W. In *Characterization of Metal and Polymer Surfaces*, Lee, L. H., Ed.; Academic Press, Inc.: New York, 1977; p 365.
(25) Napper, D. H.; Lichti, G.; Gilbert, R. G. In *Emulsion Polymers and Emulsion Polymerization*; Bassett, D. R., Hamielec, A. E., Eds.; ACS Symposium Series; American Chemical Society: Washington, DC, 1981; p 105.
(26) Flory, P. J., Ed. *Principle of Polymer Chemistry*; Cornell University Press: Ithaca, NY, 1953; p 618.
(27) Gardon, J. L. In *Polymerization Process*; Schildknecht, Skeist, Eds.; John Wiley: New York, 1977; p 143.
(28) Morawetz, H., Ed. *Macromolecules in Solution*, 2nd ed.; John Wiley: New York, 1974; Chapter 3.
(29) Hasan, S. M. *J. Polym. Sci., Polym. Chem. Ed.* **1982**, *20*, 3031.
(30) Juang, M. S.; Krieger, I. M. *J. Polym. Sci., Polym. Chem. Ed.* **1976**, *14*, 2089.
(31) Kuo, J.-F.; Chen, C.-Y. *Macromolecules* **1981**, *14*, 335.
(32) Chen, S.-A.; Lee, S.-T. *Polym. Eng. Sci.* **1985**, *25* (16), 987.
(33) Minsk, L. M.; Kotlarchik, C.; Darlak, R. S. *J. Polym. Sci., Polym. Chem. Ed.* **1973**, *11*, 353.
(34) Saini, G.; Leoni, A.; Franco, S. *Mackromol. Chem.* **1971**, *144*, 235.
(35) Currie, D. J.; Dainton, F. S.; Watt, W. S. *Polymer* **1965**, *6*, 451.
(36) Liu, L. J.; Krieger, I. M. *J. Polym. Sci., Polym. Chem. Ed.* **1981**, *19*, 3013.
(37) Hui, A. W.; Hamielec, A. E. *J. Appl. Polym. Sci.* **1972**, *16*, 749.
(38) Leonard, E. C. *Vinyl and Diene Monomers*; John Wiley & Sons: New York, 1970–1971; Parts I–III.

Registry No. St, 100-42-5; AAm, 79-06-1; KPS, 7727-21-1; (AAm)(St) (copolymer), 24981-13-3; (St)(isoprene) (copolymer), 25038-32-8.